sustainability

MDPI

Article

Case Study of Ultra-High-Performance Concrete with Urban Sludge Gasification Slag

Juntao Ma [1,*], Yanbo Huang [1], Zhiyong Li [2], Manman Yang [3], Yunfei Tan [2] and Shunbo Zhao [1]

[1] International Joint Research Lab for Eco-Building Materials and Engineering of Henan, North China University of Water Resources and Electric Power, Zhengzhou 450045, China; z202210030412@stu.ncwu.edu.cn (Y.H.); sbzhao@ncwu.edu.cn (S.Z.)
[2] Zhengzhou Sewage Purification Co., Ltd., Zhengzhou 450045, China; lizhiyonghyb@163.com (Z.L.); tanyunfei012@163.com (Y.T.)
[3] Xuchang Innovation Center of Low-Carbon Eco-Building Materials Technology, Zhongyuan Institute of Science and Technology, Zhengzhou 450042, China; yang@zykj.edu.cn
* Correspondence: majuntao@ncwu.edu.cn

Abstract: This article, for the first time, investigates the potential of Sludge Gasification Slag (SGS), a byproduct of urban sewage sludge gasification, as a lightweight aggregate in ultra-high-performance concrete (UHPC), proposing a novel sustainable solution for the utilization of SGS. The UHPC mix design followed the modified Andreasen and Andersen model, incorporating pretreated SGS, cement, silica fume (SF), river sand, and a high-efficiency water-reducing agent. A total of eight experimental groups were developed, including five pre-wetted groups (I1–I5) and three dry groups (N1–N3), to evaluate the rheological and mechanical properties of UHPC. For the first time, this study combines scanning electron microscopy (SEM) and nitrogen adsorption techniques to investigate the interfacial transition zone (ITZ) and porosity of SGS-UHPC, providing insights into the influence of SGS on the matrix. The results show that SGS, due to its irregular particle shape and high water absorption capacity, negatively impacts the flowability of the fresh mix. However, when the SGS content reached 7.5%, the plastic viscosity of the UHPC mix peaked. Notably, after 28 days of curing, the compressive strength of the 5% pre-wetted SGS group exceeded that of the control group by 5%, indicating a time-dependent strength improvement. This enhancement is primarily attributed to the water release effect of SGS, which optimizes the ITZ and strengthens the overall matrix. The findings suggest that SGS, when used at dosages below 7.5%, can be effectively incorporated into UHPC, offering a promising, environmentally friendly alternative for sustainable construction applications.

Keywords: ultra-high-performance concrete; sludge gasification slag; rheological properties; mechanical properties; microstructure; thresholding

Academic Editor: Laura Moretti

Received: 14 December 2024
Revised: 20 January 2025
Accepted: 21 January 2025
Published: 24 January 2025

Citation: Ma, J.; Huang, Y.; Li, Z.; Yang, M.; Tan, Y.; Zhao, S. Case Study of Ultra-High-Performance Concrete with Urban Sludge Gasification Slag. *Sustainability* **2025**, *17*, 938. https://doi.org/10.3390/su17030938

1. Introduction

Sludge, as a solid waste generated by urban sewage treatment plants, urgently requires treatment to address issues related to accumulation and environmental pollution. With the growing social awareness of environmental protection, attention to and exploration of sustainable development have progressively deepened. Traditional methods for urban sludge treatment face significant challenges, particularly due to their occupation of farmland and the potential for secondary pollution. This promotes the creation of a new thermal pyrolysis gasification technology for high-moisture sludge [1]. Through a process of thermal pyrolysis gasification, the sludge in a sludge pyrolysis gasifier is continuously heated in the

absence of air or in an inert atmosphere, leading to a series of physical changes at different temperatures, along with chemical reactions and the formation of products such as gases, liquids, and solids. The solids, known as sludge gasification slags (SGSs), are characterized by their lightweight, porous structure, high water absorption, and specific strength. Current research has investigated the application of SGSs in cement mortar [2,3], which demonstrates that lightweight building mortar with a dry density of less than 400 kg/m^3 can be produced with good workability, consistency, water retention, layering degree, and setting time, as well as a compressive strength no less than 3.0 MPa and a tensile adhesive strength of 0.18 MPa, with thermal conductivity in the range of 0.30–0.32 W/(m·K). This highlights the potential of using SGSs for producing ultra-high-performance concrete (UHPC), which not only helps alleviate the severe accumulation of sludge but also transforms solid waste into building materials, providing a new direction for the sustainable development of SGSs as a viable construction material.

Lightweight aggregates are widely used in construction materials, particularly for applications in thermal insulation, soundproofing, and landscaping. Their primary function is to reduce the self-weight of concrete while enhancing its durability and mechanical properties. Research has demonstrated that incorporating lightweight aggregates in appropriate proportions can significantly improve the compressive and flexural strengths of concrete [4,5]. Variations in particle morphology, pore volume, and distribution (which stem from differences in sources and production methods) can notably influence the performance of concrete [6]. Although lightweight aggregates typically exhibit lower strength compared to natural river sand, they facilitate more complete hydration of the surrounding paste, especially in the interfacial transition zone (ITZ) [7,8], thereby improving the weaker regions of the concrete matrix and enhancing overall performance [9,10]. Prewetted lightweight aggregates are an effective method to mitigate their lower strength by promoting more efficient moisture release during the hydration process, which fosters hydration reactions in the ITZ, optimizes the pore structure, and increases concrete density. Currently, lightweight aggregates are classified into natural and artificial types based on their production sources, with artificial aggregates derived from solid waste materials gaining increasing attention in recent years.

With the increasing use of lightweight and high-strength materials in construction projects, UHPC has garnered significant attention due to its exceptional mechanical properties and durability [11,12]. The strength of UHPC is influenced by various factors, including fiber content, aggregate size and grading, water-to-binder ratio, sand ratio, and superplasticizer type and dosage. To achieve optimal strength and durability, it is generally recommended to maintain a water-to-binder ratio between 0.15 and 0.25 [13]. Additionally, considering the high raw material costs associated with UHPC production and national carbon reduction strategies, incorporating solid waste as partial substitutes in UHPC can effectively reduce energy consumption while promoting the sustainable application of solid waste [14]. Researchers, including Dong et al. [15], Qing [16], and Zhang [17], have investigated the use of phosphogypsum, high-titanium slag, and iron tailings as substitutes for river sand in UHPC preparation. By employing particle packing design, various waste particles can optimize the pore structure or enhance the durability of UHPC while preserving its mechanical properties. Furthermore, Yang [18] used recycled fine aggregates to replace natural aggregates in the preparation of HPC, examining the influence of aggregate particle shape and angularity on workability. Liu [19] incorporated porous pumice into UHPC, demonstrating that the water release effect of internal curing materials in porous aggregates during the later stages of curing can compensate for early-stage development deficiencies, thereby improving later-stage strength.

The types of lightweight aggregates are diverse; however, research on the use of SGS as a lightweight aggregate in UHPC is limited. Despite the well-established use of lightweight aggregates in conventional concrete [20,21], their impact on UHPC differs significantly, and research in this area is still in its early stages [22]. Moreover, with the increasing scarcity of natural river sand, finding a low-cost and sustainable alternative to river sand has become particularly important. Therefore, investigating the performance enhancement of SGS in UHPC and the sustainable utilization of sludge is of significant importance. After crushing and sieving the SGS, particles within the size ranges of 0–0.6 mm and 0.6–1.18 mm are selected to replace river sand [23]. Based on the analysis of particle size distribution, shape, and water absorption rate, the modified Andreasen and Andersen (M-A&A) model is employed to design the mix proportions. Different pre-wetting methods are applied based on the water absorption rate of the particles, and UHPC is prepared. The study investigates the effect of particle shape and water absorption characteristics on the rheological and mechanical properties of UHPC. Furthermore, the research combines microscopic morphology, porosity, and pore distribution analyses to explore the mechanism and feasibility of utilizing SGS in UHPC preparation.

2. Experimental Work

2.1. Character of SGS

2.1.1. Chemical Composition and Morphology

The SGS used in this experiment was obtained from the residue of pyrolysis gasification at the Zhengzhou Municipal Sewage Treatment Plant. Crushing was performed using a laboratory-scale jaw crusher, and particles with sizes ranging from 0 to 0.6 mm and 0.6 to 1.18 mm were sieved, yielding apparent densities of 2160 kg/m^3 and 2020 kg/m^3, respectively. The chemical compositions of the SGS, cement, and silica fume (SF) used in this study are presented in Table 1. Figure 1 shows the X-ray diffraction pattern and SEM microstructure of SGS, revealing quartz and feldspar as the primary mineral phases. The image in Figure 2 illustrates the porous structure of SGS, with pore sizes highlighted using yellow markers. The pore diameters are predominantly distributed between 5 and 105 μm.

Table 1. Chemical composition of raw materials (wt.%).

Chemical Composition	SiO_2	Al_2O_3	Fe_2O_3	MgO	CaO	Na_2O	K_2O	MnO	LOI
SGS	47.27	15.23	4.66	3.65	7.31	1.48	2.14	0.1	5.76
SF	97.51	0.16	-	0.88	0.38	0.33	0.29	-	0.20
Cement	20.86	5.90	3.61	3.50	56.77	-	-	-	1.16

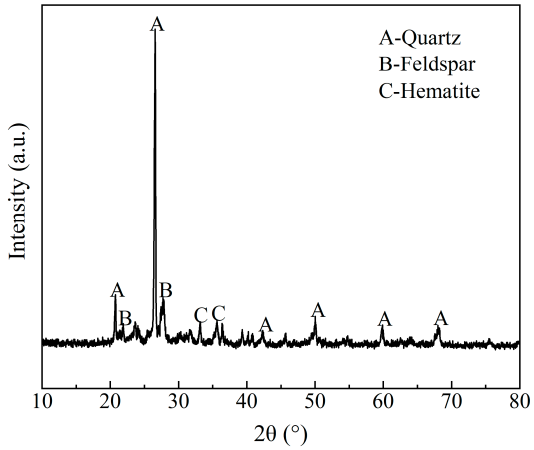

Figure 1. X-ray diffraction pattern of SGS.

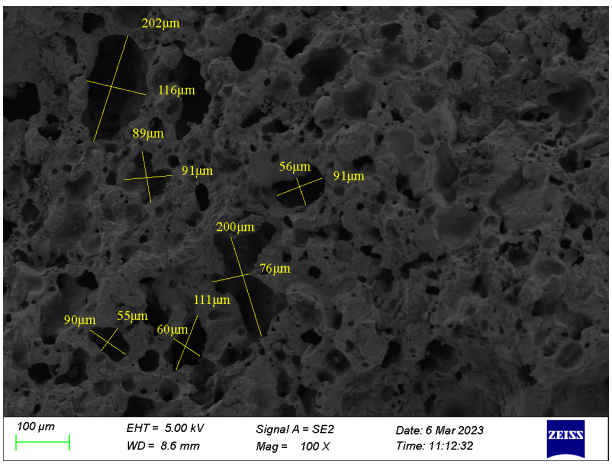

Figure 2. SEM microstructure of SGS.

2.1.2. Particle Size and Shape Analysis

The particle size distribution and shape of SGS aggregates were analyzed using the Occhio Scan 700 particle size and shape analyzer (Xinlong Building, Jiancaiceng West Road, Beijing, China). The distribution curves for different particle size ranges are shown in Figure 3. The particle shapes of the 0–1.18 mm fractions were compared with those of ordinary river sand, with the scanning images and shape analysis presented in Figures 4 and 5. According to the particle size distribution curve, particles in the 0–0.6 mm range are primarily concentrated below 0.2 mm, while the distribution of particles in the 0.6–1.18 mm range is more uniform. In terms of particle shape, SGS aggregates exhibit a rougher surface with more pronounced angularity compared to river sand, and internal porosity within the particles was also observed. Based on the scanning images, the bluntness parameter was calculated for quantitative analysis of particle morphology (Figure 5). The equivalent volume peak ratio for SGS corresponds to a bluntness of 40%, whereas the equivalent volume peak ratio for river sand corresponds to a bluntness of 65%. This indicates that SGS aggregates have a lower overall bluntness compared to river sand, suggesting that river sand has a smoother surface and a shape closer to a sphere, while SGS aggregates consist of more angular particles with relatively sharp boundaries.

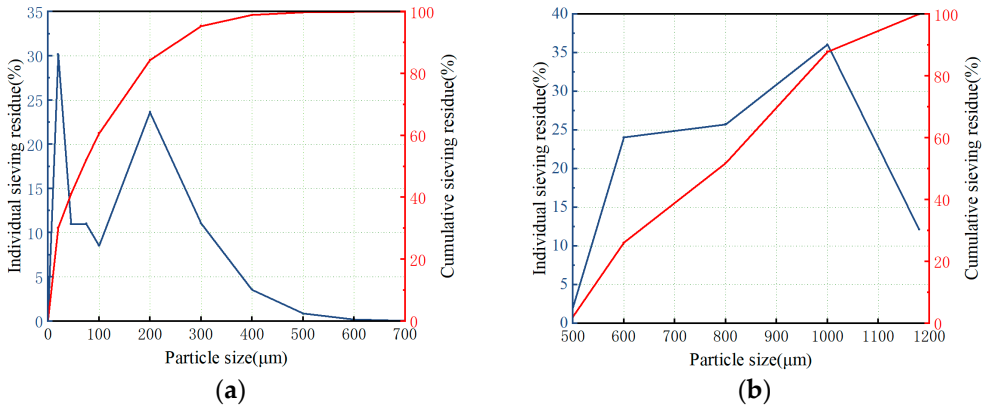

Figure 3. SGS distribution curve: (**a**) SGS distribution curve for 0–0.6 mm, (**b**) SGS distribution curve for 0.6–1.18 mm.

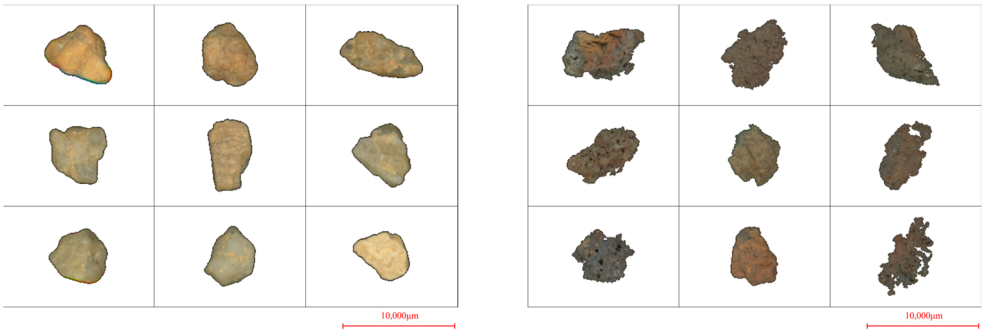

Figure 4. Scanning electron microscopy image of 0–1.18 mm river sand and SGS particles: (**a**) river sand, (**b**) SGS.

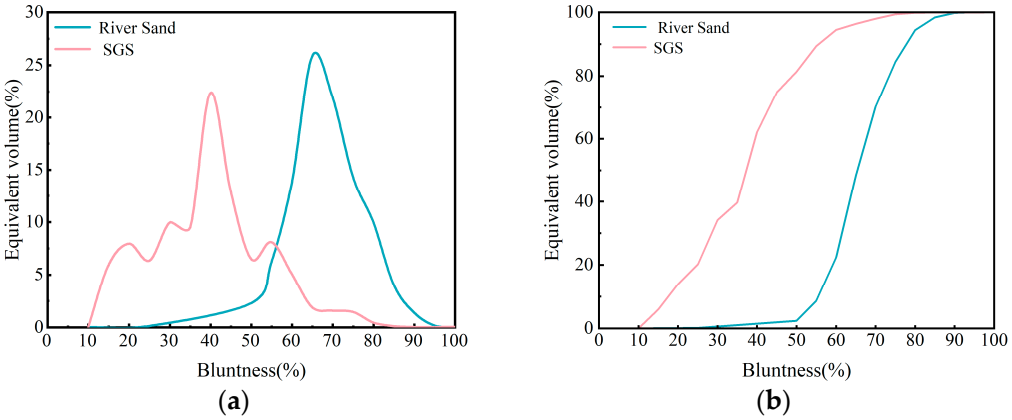

Figure 5. Equivalent volume distribution curve with bluntness of 0–1.18 mm river sand and SGS: (**a**) dividing curve, (**b**) cumulative curve.

2.1.3. Water Absorption Rate

The water absorption rate test was conducted in accordance with the provisions of the Chinese standard GB/T 14684-2022 [24]. After drying the river sand (Sand1 and Sand2) and SGS aggregates (SGS1 and SGS2) to a constant weight, the samples were pre-wetted by immersion in water and then air-dried to a saturated surface-dry state using an air blower. The water absorption rates were measured at 1 h and 24 h (Table 2). SGS2 exhibited water absorption rates of 16.45% at 1 h and 21.31% at 24 h, which were significantly higher than those of ordinary river sand.

Table 2. Water absorption rate (WAR) of river sand and SGS.

Materials	Sand1	Sand2	SGS1	SGS2
1 h WAR (%)	1.09	1.05	2.03	16.45
24 h WAR (%)	1.12	1.08	2.16	21.31

2.2. Properties of Other Raw Materials

P·O 52.5 cement with a specific surface area of 381 m^2/kg and a density of 2230 kg/m^3, along with SF, were used as the cementitious materials in this study. A powdered polycarboxylate-based superplasticizer was employed as the water-reducing agent. River sand sourced from the Yutang River in Henan Province was selected and sieved into two particle size ranges, 0–0.6 mm and 0.6–1.18 mm, with apparent densities of 2580 kg/m^3 and 2590 kg/m^3, respectively.

2.3. Mix Proportion Design of UHPC

The mix design was based on a modified Andreasen and Andersen (M-A&A) model [25,26] (Figure 6). Using the particle size distributions of cement, SF, river sand, and SGS (with particle sizes of 0–0.6 mm and 0.6–1.18 mm), the mix proportions were determined through particle packing design. A control group was included for comparison, as detailed in Table 3. The control group is denoted as M0, while groups I1–I5 represent the pre-wetted groups, where SGS replaces river sand at replacement rates of 5%, 7.5%, 10%, 12.5%, and 15%, respectively. Groups N1–N3 represent the dry groups, where SGS replaces river sand at replacement rates of 5%, 7.5%, and 10%, respectively. PW indicates pre-wetted water. The mix design ensured a consistent water-to-cement ratio, with the moisture content of the pre-wetted portion incorporated into the total water-to-cement ratio. The SGS images for the 0–0.6 mm and 0.6–1.18 mm particle size ranges are shown in Figure 7.

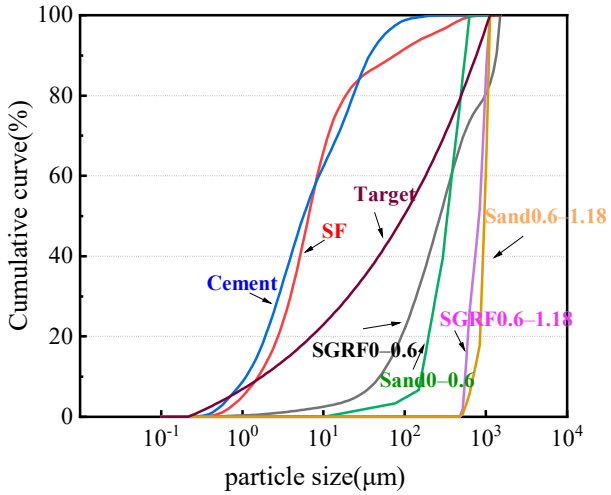

Figure 6. Particle size distribution of raw materials and target curve.

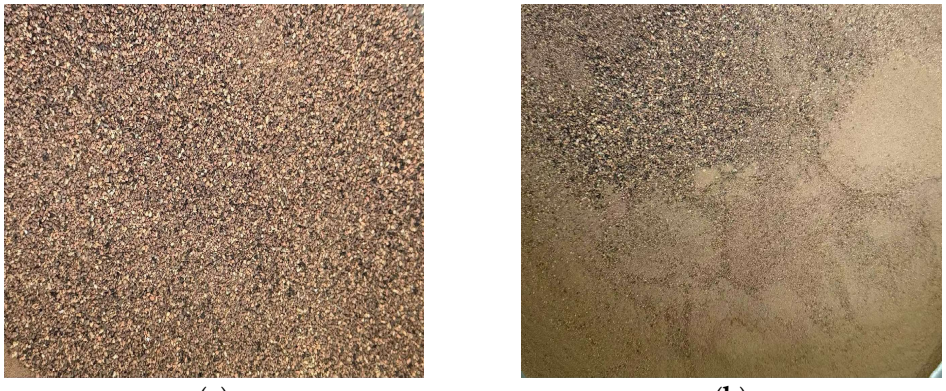

(**a**) (**b**)

Figure 7. The SGS images of the 0–0.6 mm and 0.6–1.18 mm particle size ranges: (**a**) 0.6–1.18 mm, (**b**) 0–0.6 mm.

Table 3. Mix proportion design for UHPC (kg/m^3).

Sample	Cement	SF	Sand1	Sand2	SGS1	SGS2	Water	PW	Water Reducer (wt.%)
M0	1244	112	1162.0	259.0	-	-	224.0	-	3%
I1	1244	112	1103.9	246.0	58.1	13.0	221.9	2.1	3%
I2	1244	112	1074.8	239.6	87.2	19.4	220.8	3.2	3%

Table 3. *Cont.*

Sample	Cement	SF	Sand1	Sand2	SGS1	SGS2	Water	PW	Water Reducer (wt.%)
I3	1244	112	1045.8	233.1	116.2	25.9	219.7	4.3	3%
I4	1244	112	1016.7	226.6	145.3	32.4	218.7	5.3	3%
I5	1244	112	987.7	220.1	174.3	38.9	217.6	6.4	3%
N1	1244	112	1103.9	246.0	58.1	13.0	224.0	-	3%
N2	1244	112	1074.8	239.6	87.2	19.4	224.0	-	3%
N3	1244	112	1045.8	233.1	116.2	25.9	224.0	-	3%

2.4. Test Methods

The flowability of the freshly mixed UHPC was evaluated using a flowability test conducted in accordance with Chinese standard GB/T 2419-2005 [27]. The rheological properties of the freshly mixed UHPC were examined with an American BROOKFIELD RST-SST rheometer, as shown in Figure 8. The prepared UHPC was placed in a 250 mL beaker, and the slurry was poured into the beaker until it reached a volume of 200 mL. A VT-40–20 rotor was employed to conduct the test at a temperature of (20 ± 0.5) °C. The rheological properties were analyzed using the descent curve method [28,29]. The testing procedure is illustrated in Figure 9. The maximum shear rate was set to 25 s^{-1} [22], and the test duration was 195 s, divided into pre-shearing and formal shear stages. Pre-shearing was performed at a constant shear rate of 25 s^{-1} for 60 s, followed by a 15 s pause before the formal shear commenced. The shear rate increased from 0 s^{-1} to 25 s^{-1} within 60 s and then decreased back to zero over another 60 s.

Figure 8. RST-SST rheometer.

In the evaluation of the hardened UHPC performance, compressive and flexural strength tests were conducted after curing under standard conditions for 3 and 28 days. The testing methods adhered to the requirements outlined in Chinese standard GB/T 17671-2021 [30]. The mechanical property testing equipment is shown in Figure 10. Additionally, the microstructure of UHPC samples with different proportions, cured for 28 days, was observed using the Zeiss Gemini Sigma 300 scanning electron microscope (Carl Zeiss AG, Oberkochen, Germany) (Figure 11). Their pore characteristics were analyzed using the PS-1547 porosimeter (nitrogen adsorption method) from Beijing Betters Instrument Technology Co., Ltd., Beijing, China (Figure 12).

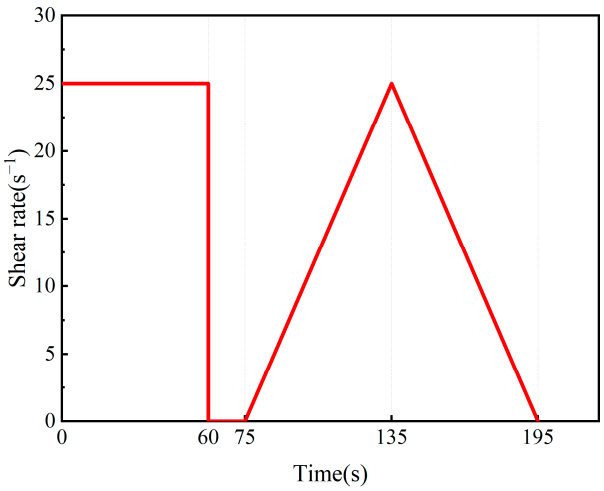

Figure 9. Rheological test program.

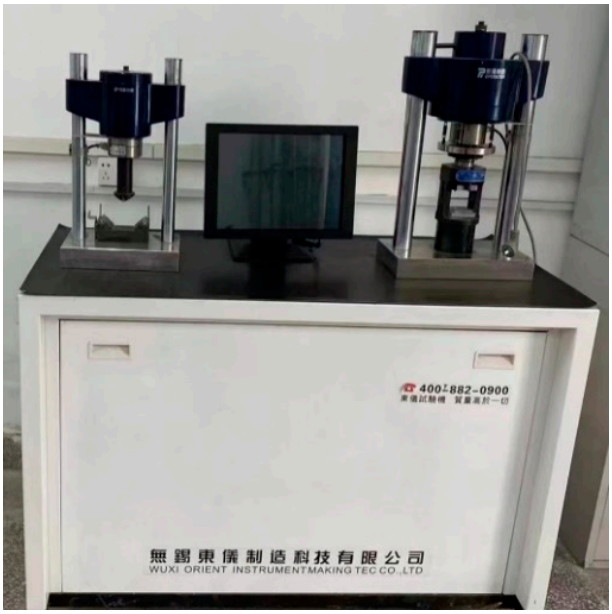

Figure 10. Anti-bending compression machine.

Figure 11. Scanning electron microscope.

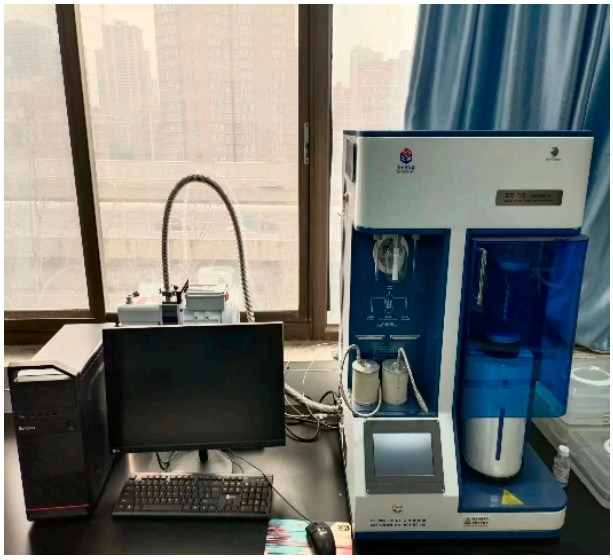

Figure 12. Accelerated surface area and porosimetry system.

3. Results and Analyses

3.1. Rheological Properties of Fresh UHPC

The flowability test results for freshly mixed UHPC with varying proportions are presented in Figure 13. The slump flow of the mixture without the SGS additive was 190 mm, whereas the inclusion of SGS led to a decrease in mortar flowability. As the SGS content increased from 5% (I1) to 15% (I5), a significant reduction of approximately 31.6% in flowability was observed. Compared to the dry group, the pre-wetted group exhibited a less pronounced decrease in flowability. This suggests that, under identical total water-to-binder ratio conditions (excluding the water used for pre-wetted), the mortar in the dry group contained more free water than in the pre-wetted group. However, during hydration, some of the excess water in the dry group infiltrated into the interior of SGS particles, consuming a portion of the free water, which resulted in a decrease in flowability compared to the control group but still higher than that in the pre-wetted groups.

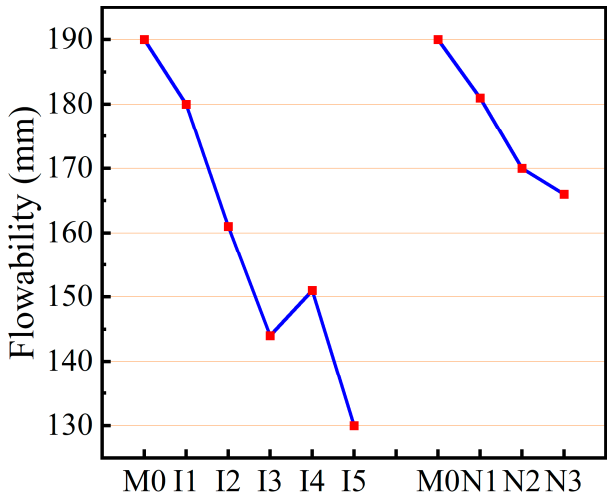

Figure 13. Fluidity of fresh UHPC.

Figure 14 shows the comparison of rheological curves for freshly mixed UHPC with different proportions. The data were fitted using the Modified Bingham Model. The fitting equation for the Modified Bingham Model is expressed as follows:

$$\tau = \tau_0 + \mu\gamma + c\gamma^2, \tau \geq \tau_0 \quad (1)$$

The τ represents the shear stress (Pa), τ_0 denotes the yield stress (Pa), μ stands for the plastic viscosity (Pa·s), γ represents the shear rate (s^{-1}), and c is the coefficient ($Pa \cdot s^2$). Figure 15 displays the results of the fitted plastic viscosity (μ) and yield stress (τ_0).

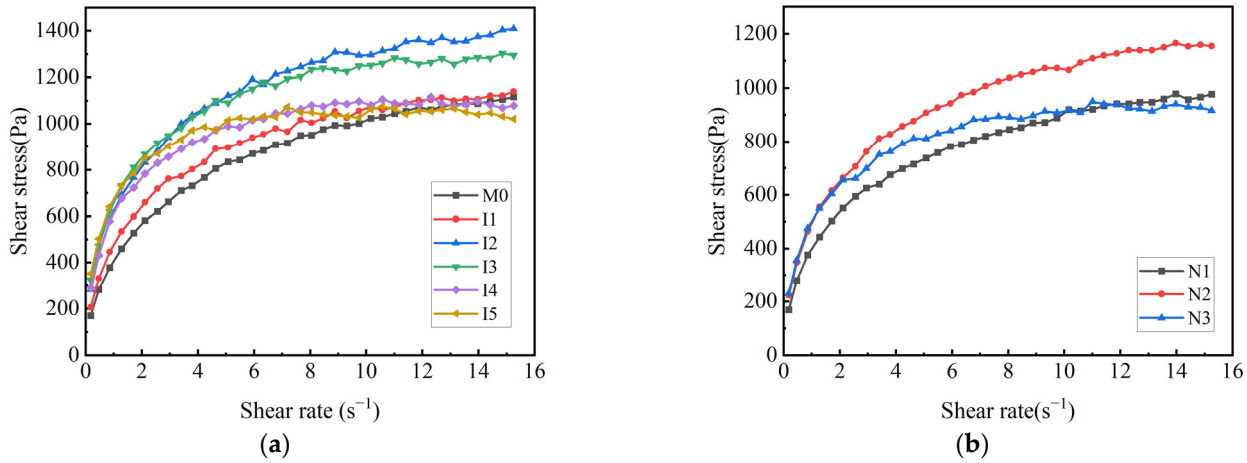

Figure 14. Rheological curve of UHPC: (**a**) groups M0 and I1~I5, (**b**) groups M0 and N1~N3.

From Figure 15, it is evident that the yield stress exhibits an increasing trend with the augmentation of SGS content. In comparison, the dry group demonstrates relatively lower yield stress and plastic viscosity than the pre-wetted group. By comparing plastic viscosity values at different contents, it can be observed that when the content of pre-wetted SGS reaches 7.5%, there is a peak in plastic viscosity, indicating a 22.5% increase compared to the control group. As the content further increases, plastic viscosity starts to decline and reaches a minimum value of 105.87 Pa·s, which is 14.4% lower than that of the blank group. This suggests that the incorporation of SGS leads to a continuous enhancement in UHPC's yield stress while exhibiting an initial increment followed by a decrement in plastic viscosity.

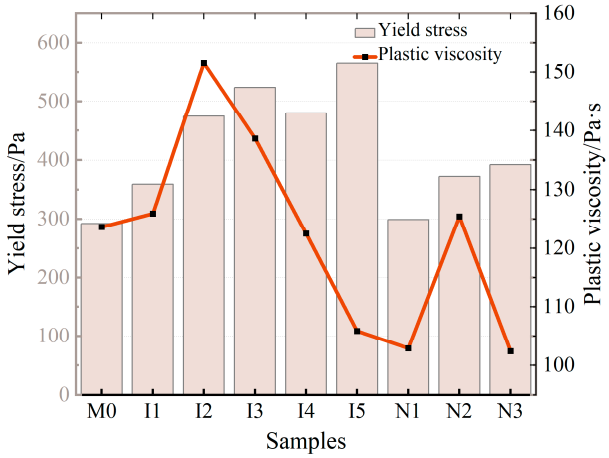

Figure 15. Yield stress and plastic viscosity of fresh UHPC.

Figure 16 presents an idealized diagram illustrating the rheological mechanism of SGS-modified UHPC, where the rheological performance of fresh UHPC is directly influenced by the particle morphology and water absorption characteristics of the added SGS. The angular shape of SGS particles, with a bluntness of approximately 60% that of river sand, results in higher frictional forces between particles and increased resistance during slurry

flow compared to the smoother river sand. Additionally, the porous nature of SGS leads to a larger specific surface area than the river sand, creating a thinner average water film on particle surfaces, which subsequently reduces the flowability of UHPC [31]. Furthermore, pre-wetted SGS particles exhibit lower moisture content in the cement slurry compared to the dry group under identical total water-to-binder ratio conditions, leading to relatively poorer rheological performance. In contrast, untreated SGS particles absorb some moisture from the cement slurry, reducing free water content and consequently decreasing flowability. At 10% SGS content and a shear rate of 10 s^{-1}, the mortar yield stress exceeds that of the non-replaced samples, while plastic viscosity significantly decreases, indicating the opening of the structure among nested SGS particles at higher shear rates, thereby reducing flow resistance and enhancing flowability. Figure 17 depicts a linear relationship between yield stress and flowability for freshly mixed UHPC at different proportions, showing a well-defined correlation with a gradual decrease in yield stress as flowability increases. As the SGS content gradually increases, both yield stress and flowability decrease, with this trend becoming more pronounced at higher contents.

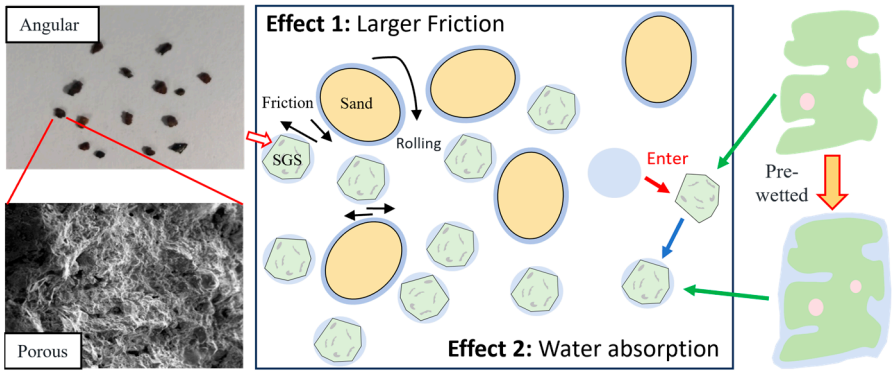

Figure 16. Rheological mechanism schematic of SGS-UHPC.

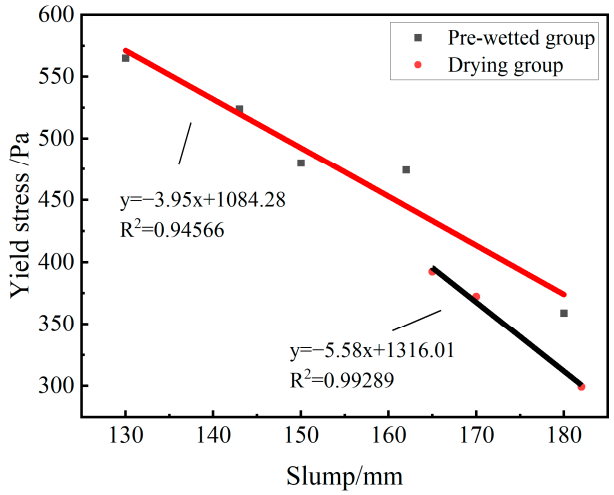

Figure 17. Relationship between flowability and yield stress of the pre-wetted group and dry group.

3.2. Mechanical Properties of UHPC

The compressive and flexural strength test results of UHPC with varying proportions after curing for 3 days and 28 days are shown in Figure 18. Compared to the M0 sample without SGS addition, the I1 sample containing 5% pre-wetted SGS exhibited a slight reduction in early strength but demonstrated an approximate 5% increase in compressive strength at 28 days. In contrast, the addition of the same amount of untreated SGS showed no significant enhancement in later-stage strength, indicating that pre-wetted SGS positively

contributes to the hydration process of cementitious materials in UHPC and facilitates strength development. However, as the SGS content increased further, the improvement trend diminished and began to decline, suggesting that the intrinsic strength of SGS is lower than that of river sand. Excessive incorporation of SGS leads to aggregate self-destruction, which becomes a dominant factor, resulting in reduced compressive and flexural strengths.

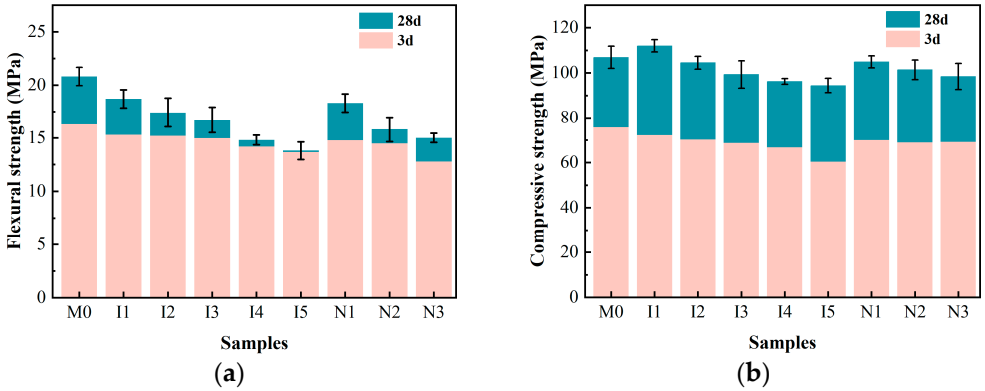

Figure 18. The mechanical performance testing of UHPC: (**a**) compressive strength, (**b**) flexural strength.

The study introduced the compressive strength enhancement rate to assess the strength development of UHPC from 3 days to 28 days (Figure 19), with the M0 group designated as the control group, red represents the intensity of growth relative to M0, while blue represents the intensity of decline relative to M0. The compressive strength enhancement rate for each group was determined by calculating the difference in strength growth between each group and the M0 group. It is evident that, during the period from 3 days to 28 days, the pre-wetted groups with less than 10% content exhibit significantly higher strength growth compared to the dry group. Moreover, when reaching a content of 10%, only a relatively minor decline in strength growth was observed in the pre-wetted groups, thus confirming the water release effect of pre-wetted SGS in UHPC.

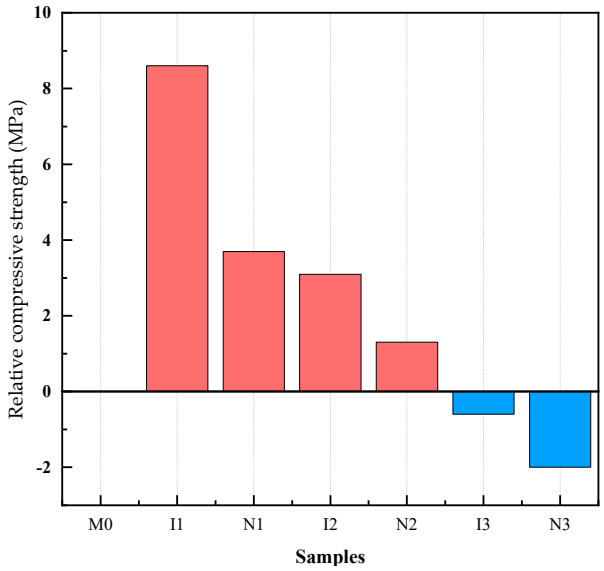

Figure 19. The compressive strength enhancement rate of UHPC.

3.3. Microstructures of UHPC

3.3.1. Microstructural Observation

After 28 days of curing, scanning electron microscopy was employed to conduct microstructural analysis on the pre-wetted groups I1 and I3, as well as the dry groups N1

and N3, as illustrated in Figure 20. A comparative evaluation revealed that the ITZ of specimens I1 and I3, which incorporated pre-wetted SGS, exhibited favorable contact with the matrix. In contrast, noticeable cracks and voids were observed in the interface transition zones surrounding dry groups N1 and N3. This suggests that during the later stages of hydration in UHPC, the moisture provided by saturated pre-wetted SGS adequately facilitated thorough hydration of the interface transition zones within the pre-wetted group. Consequently, this improved density of hydration products within these regions promoted strength development in UHPC during subsequent stages. Examination of hydration products within the interface transition zone indicated a significant presence of amorphous C-S-H gel, AFt, along with a small amount of $Ca(OH)_2$ crystals in the pre-wetted group. The water released by SGS facilitated secondary hydration reactions involving SF particles adjacent to it while consuming CH crystals present in ITZ. Moreover, a substantial quantity of amorphous C-S-H gel filled both pores within the interface area and those inside SGS particles. Conversely, unhydrated particles were still evident in specimens from dry groups, indicating comparatively lower levels of hydration compared to their counterparts from pre-wetted groups, resulting in relatively poor density.

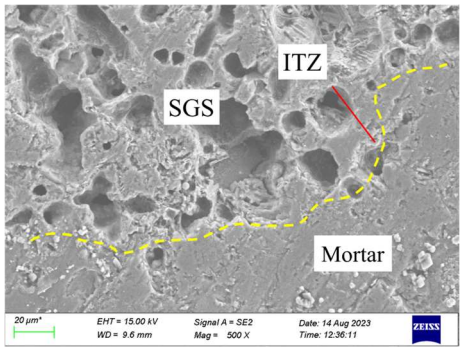

(**a**) I1 (500×)

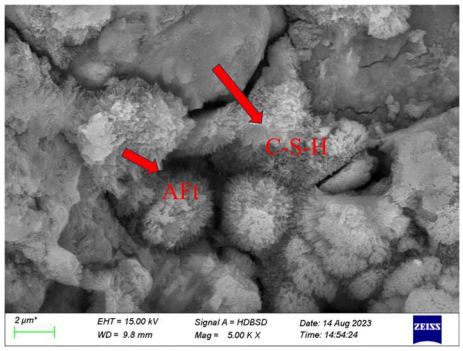

(**b**) I1 (5000×)

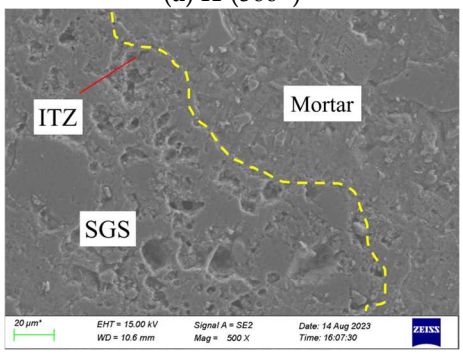

(**c**) I3 (500×)

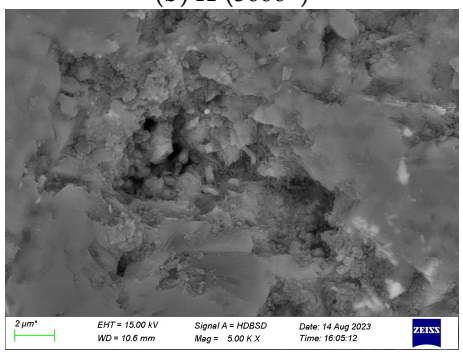

(**d**) I3 (5000×)

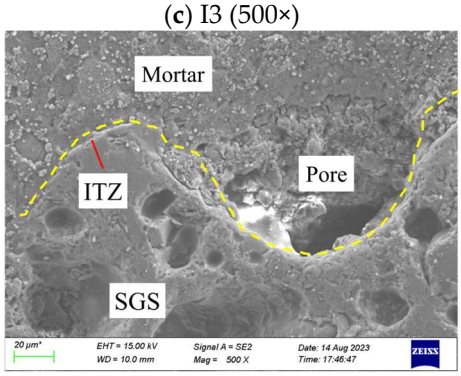

(**e**) N1 (500×)

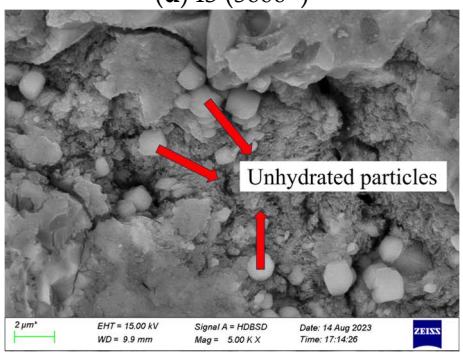

(**f**) N1 (5000×)

Figure 20. *Cont.*

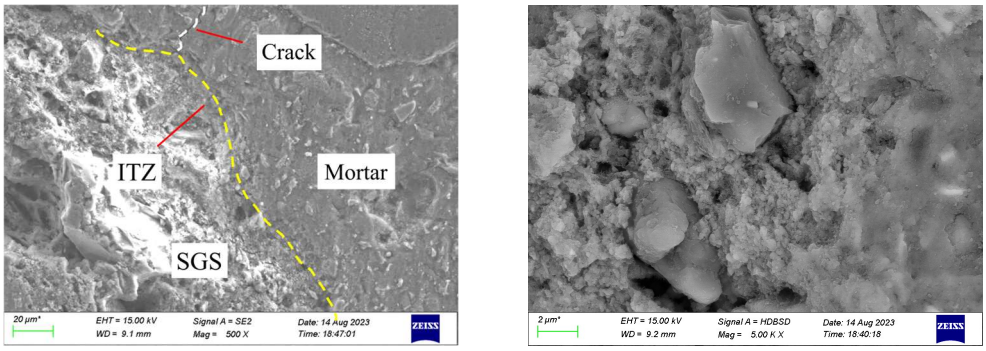

(**g**) N3 (500×) (**h**) N3 (5000×)

Figure 20. Different mix of UHPC after 28 days of curing micromorphology.

3.3.2. Analysis of Porosity Characteristics in UHPC

The pore structure of UHPC specimens cured for 28 days with different proportions was analyzed using the nitrogen adsorption method, and the resulting pore distribution curves are presented in Figure 21. All UHPC groups exhibited hysteresis loops in their adsorption isotherms, indicating capillary condensation of internal pores during desorption. According to the classification by the International Union of Pure and Applied Chemistry (IUPAC) [32,33], these isotherms can be classified as type H3, which signifies unsaturated adsorption at high pressure and suggests the presence of slit-shaped mesopores and macropores [34]. Most of the pores in different specimens were found to be distributed within the micropore range, predominantly below 8nm, with some additional pores observed in the range of 20~50 nm. Based on Wu's classification of pores [35], it can be concluded that each UHPC group primarily consists of innocuous pores (<20 nm) and slightly harmful pores (20~50 nm). The percentage distribution of pores in each UHPC group is shown in Figure 22. For pre-wetted and dry groups, those with a higher SGS content (I3 and N3) exhibited higher porosity across all pore size ranges. Furthermore, pre-wetted significantly improved the level of harmful pores in pre-wetted specimens by reducing them by 52.76% (at 5% content) and 8.2% (at 10% content), indicating that pre-wetted can refine pore size and prevent detrimental pore development. It is evident that pre-wetted SGS has the potential to optimize pore characteristics in SGS-added UHPC, thereby enhancing its mechanical properties.

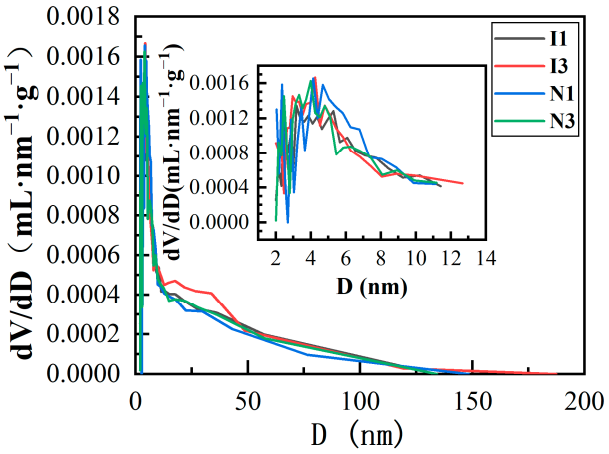

Figure 21. Pore size distribution curve of UHPC (nitrogen adsorption).

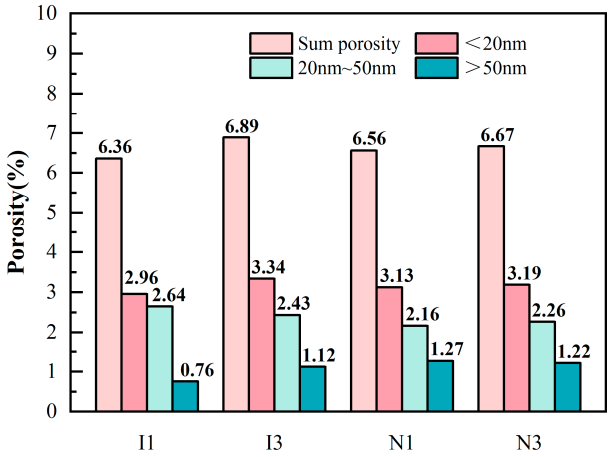

Figure 22. Pore classification proportion of UHPC.

4. Conclusions

The rheological properties, mechanical performance, and microstructure of UHPC prepared by partially replacing river sand with SGS were analyzed. The main findings are as follows:

(1) The flowability of fresh UHPC decreases with the addition of SGS, particularly in the dry mix with consistent total water content. For pre-wetted SGS, the plastic viscosity of UHPC peaks at a 7.5% dosage, while the yield stress continues to increase as the SGS content increases.

(2) Incorporating 5% pre-wetted SGS enhances the 28-day compressive strength of UHPC by approximately 5%. However, further increases in SGS dosage lead to predominant damage to the aggregates themselves, causing a decrease in both compressive and flexural strengths. This can be attributed to the lower intrinsic strength of SGS, which reduces the overall strength of the UHPC. Notably, UHPC containing pre-wetted SGS exhibits significantly superior mechanical performance compared to those without.

(3) The incorporation of pre-wetted SGS during cement hydration optimizes the interfacial structure of UHPC due to its water release effect. Compared to the non-replaced specimens, the addition of 5% pre-wetted SGS reduces the harmful pore volume in UHPC by 52.76%.

(4) The experimental results show that pre-wetted SGS, with a dosage of up to 7.5%, can be effectively incorporated into UHPC, especially at a 5% dosage. The mechanism involves the release of water from the pre-wetted SGS during the hardening process of UHPC (from 7 to 28 days), which promotes secondary hydration of the unhydrated cement, SF, and $Ca(OH)_2$ in the ITZ between the mortar and SGS. This secondary hydration generates significant amounts of C-S-H gel, which fills internal pores and densifies the weakest regions of the UHPC, ultimately enhancing its overall strength.

Author Contributions: Writing—original draft, Y.H.; Methodology, J.M.; Data curation, J.M., Y.H., Z.L. and M.Y.; Formal analysis, Y.H.; Writing—review and editing, J.M.; Supervision, Y.T. and S.Z. All authors have read and agreed to the published version of the manuscript.

Funding: This study was funded by the National Natural Science Foundation of China (51508191), the Science and Technology Project of Henan Province (242102321058), the Key Scientific Research Project of Henan University (24A560027), and the Colleges Young Teacher Training Project of Henan Province (2023GGJS074).

Institutional Review Board Statement: Not applicable.

Informed Consent Statement: Informed consent was obtained from all subjects involved in the study.

Data Availability Statement: The original contributions presented in this study are included in the article.

Acknowledgments: This research has benefited from the experts and laboratory manager of the International Joint Research Lab for Eco-building Materials and Engineering of Henan.

Conflicts of Interest: Author Zhiyong Li and Yunfei Tan was employed by the company Zhengzhou Sewage Purification Co., Ltd., The remaining authors declare that the research was conducted in the absence of any commercial or financial relationships that could be construed as a potential conflict of interest.

References

1. *TCAMIE 10-2022*; Standard for Pyrolysis Gasification Technology of Sludge from Urban Sewage Treatment Plant. Beijing Sci-Tech Press: Beijing, China, 2023.
2. Li, C.; Zhang, X.; Zhang, B.; Tan, Y.; Li, F. Reuse of sintered sludge from municipal sewage treatment plants for the production of lightweight aggregate building mortar. *Crystals* **2021**, *11*, 999. [CrossRef]
3. Zhang, X.; Zhang, B.; Liang, N.; Tan, Y.; Zhao, S. Experimental study on the feasibility of municipal sewage treatment sintered sludge used for building fine aggregate. *N. Build. Mater.* **2021**, *48*, 103.
4. Meng, W.; Khayat, K. Effects of saturated lightweight sand content on key characteristics of ultra-high-performance concrete. *Cem. Concr. Res.* **2017**, *101*, 46–54. [CrossRef]
5. Liu, K.; Yu, R.; Shui, Z.; Li, X.; Ling, X.; He, W.; Yi, S.; Wu, S. Effects of pumice-based porous material on hydration characteristics and persistent shrinkage of ultra-high performance concrete (UHPC). *Materials* **2018**, *12*, 11. [CrossRef]
6. Fořt, J.; Afolayan, A.; Medved', I.; Scheinherrová, L.; Černý, R. A review of the role of lightweight aggregates in the development of mechanical strength of concrete. *J. Build. Eng.* **2024**, *89*, 109312. [CrossRef]
7. Liu, J.; Shi, C.; Farzadnia, N.; Ma, X. Effects of pretreated fine lightweight aggregate on shrinkage and pore structure of ultra-high strength concrete. *Constr. Build. Mater.* **2019**, *204*, 276–287. [CrossRef]
8. Li, S.; Jensen, O.; Wang, Z.; Yu, Q. Influence of micromechanical property on the rate-dependent flexural strength of ultra-high performance concrete containing coarse aggregates (UHPC-CA). *Compos. Part B Eng.* **2021**, *227*, 109394. [CrossRef]
9. Bentz, D.; Geiker, M.; Hansen, K. Shrinkage-reducing admixtures and early-age desiccation in cement pastes and mortars. *Cem. Concr. Res.* **2001**, *31*, 1075–1085. [CrossRef]
10. Trtik, P.; Münch, B.; Weiss, W.; Kaestner, A.; Jerjen, I.; Josic, L.; Lehmann, E.; Lura, P. Release of internal curing water from lightweight aggregates in cement paste investigated by neutron and X-ray tomography. *Nucl. Instrum. Methods Phys. Res. Sect. A Accel. Spectrometers Detect. Assoc. Equip.* **2011**, *651*, 244–249. [CrossRef]
11. Amran, M.; Huang, S.; Onaizi, A.; Makul, N.; Abdelgader, H.S.; Ozbakkaloglu, T. Recent trends in ultra-high performance concrete (UHPC): Current status, challenges, and future prospects. *Constr. Build. Mater.* **2022**, *352*, 129029. [CrossRef]
12. Shao, X.; Qiu, M.; Yan, B.; Luo, J. A review on the research and application of ultra-high performance concrete in bridge engineering around the world. *Mater. Rep.* **2017**, *31*, 33–43.
13. Shi, C.; Wu, Z.; Xiao, J.; Wang, D.; Huang, Z.; Fang, Z. A review on ultra high performance concrete: Part I. Raw materials and mixture design. *Constr. Build. Mater.* **2015**, *101*, 741–751. [CrossRef]
14. Du, J.; Meng, W.; Khayat, K.H.; Bao, Y.; Guo, P.; Lyu, Z.; Abu-Obeidah, A.; Nassif, H.; Wang, H. New development of ultra-high-performance concrete (UHPC). *Compos. Part B Eng.* **2021**, *224*, 109220. [CrossRef]
15. Dong, E.; Fu, S.; Wu, C.; Lv, W.; Liu, X.; Zhang, L.; Feng, Y.; Shui, Z.; Yu, R. Value-added utilization of phosphogypsum industrial by-products in producing green Ultra-High performance Concrete: Detailed reaction kinetics and microstructure evolution mechanism. *Constr. Build. Mater.* **2023**, *389*, 131726. [CrossRef]
16. Qing, T. Design and Performances of Ultra-High Performance Concrete Based on High Titanium Slag. Master's Thesis, Southwest University of Science and Technology, Mianyang, China, 2023.
17. Zhang, W.; Gu, X.; Qiu, J.; Liu, J.; Zhao, Y.; Li, X. Effects of iron ore tailings on the compressive strength and permeability of ultra-high performance concrete. *Constr. Build. Mater.* **2020**, *260*, 119917. [CrossRef]
18. Yang, C. Characterization of Mechanical Sand Grain Shape Parameters and Their Influence on the Properties of High-performance Concrete. Master's Thesis, Chongqing Jiaotong University, Chongqing, China, 2023.
19. Liu, K. Study on Volume Stability Evolution Mechanism and Regulation Technology of Ultra-High Performance Concrete Incorporating Porous Internal Curing Agent. Ph.D. Thesis, Wuhan University of Technology, Wuhan, China, 2020.
20. Mo, K.; Ling, T.; Alengaram, U.; Yap, S.; Yuen, C. Overview of supplementary cementitious materials usage in lightweight aggregate concrete. *Constr. Build. Mater.* **2017**, *139*, 403–418. [CrossRef]
21. Alqahtani, F.; Zafar, I. Plastic-based sustainable synthetic aggregate in Green Lightweight concrete—A review. *Constr. Build. Mater.* **2021**, *292*, 123321. [CrossRef]

22. Ding, Q.; Guo, K.; Cheng, H.; Zhang, G. Research Progress of Lightweight Aggregate in Ultra-high Performance Concrete. *J. Build. Mater.* **2023**, *26*, 886.
23. Liu, K.; Yu, R.; Shui, Z.; Yi, S.; Li, X.; Ling, G.; He, Y. Influence of external water introduced by coral sand on autogenous shrinkage and microstructure development of Ultra-High Strength Concrete (UHSC). *Constr. Build. Mater.* **2020**, *252*, 119111. [CrossRef]
24. *GB/T 14684-2022*; State Administration for Market Regulation: Sand for Construction. Standards Press of China: Beijing, China, 2022.
25. Yu, R.; Spiesz, P.; Brouwers, H. Mix design and properties assessment of ultra-high performance fiber reinforced concrete (UHPFRC). *Cem. Concr. Res.* **2014**, *56*, 29–39. [CrossRef]
26. Wang, X.; Yu, R.; Shui, Z.; Song, Q.; Zhang, Z. Mix design and characteristics evaluation of an eco-friendly Ultra-High Performance Concrete incorporating recycled coral based materials. *J. Clean. Prod.* **2017**, *165*, 70–80. [CrossRef]
27. *GB/T 2419-2005*; The State Bureau of Quality and Technical Supervision: Test Method for Fluidity of Cement Mortar. Standards Press of China: Beijing, China, 2005.
28. Ehsani, A.; Nili, M.; Shaabani, K. Effect of nanosilica on the compressive strength development and water absorption properties of cement paste and concrete containing Fly Ash. *KSCE J. Civ. Eng.* **2017**, *21*, 1854–1865. [CrossRef]
29. Cao, R.; Zhou, M.; Zhou, Q.; He, Y. Effect of ultra-fine fly ash on rheological properties, mechanical properties and microstructure of ultra-high performance concrete. *Mater. Rep.* **2019**, *33*, 2684.
30. *GB/T 17671-2021*; The State Bureau of Quality and Technical Supervision: Test Method of Cement Mortar Strength (ISO Method). Standards Press of China: Beijing, China, 2021.
31. Liu, Y.; Wu, Z.; Zhang, X.; Shi, C. Rheological Properties and Their Regulation of Ultra-High Performance Concrete—A Short Review. *J. Chin. Ceram. Soc.* **2023**, *51*, 3025.
32. Brunauer, S.; Deming, L.; Deming, W.; Teller, E. On a theory of the van der Waals adsorption of gases. *J. Am. Chem. Soc.* **1940**, *62*, 1723–1732. [CrossRef]
33. Thommes, M.; Kaneko, K.; Neimark, A.; Olivier, J.P.; Rodriguez-Reinoso, F.; Rouquerol, J.; Sing, K.S.W. Physisorption of gases, with special reference to the evaluation of surface area and pore size distribution (IUPAC Technical Report). *Pure Appl. Chem.* **2015**, *87*, 1051–1069. [CrossRef]
34. Peng, N. Pore Structure and Fractal Characteristics of Wufeng and Lower Member of Longmaxi Shales in Western Hubei and Eastern Chongqing Regions. Ph.D. Thesis, China University of Geosciences, Wuhan, China, 2019.
35. Wu, Z.; Lian, H. *High Performance Concrete*; China Railway Publishing House: Beijing, China, 1999; p. 24.